World Academy of Science, Engineering and Technology
International Journal of Mechanical and Mechatronics Engineering
Vol:11, No:6, 2017

Empirical Heat Transfer Correlations of Finned-Tube Heat Exchangers in Pulsatile Flow

Jason P. Michaud, Connor P. Speer, David A. Miller, David S. Nobes

Abstract**—**An experimental study on finned-tube radiators has been conducted. Three radiators found in desktop computers sized for 120 mm fans were tested in steady and pulsatile flows of ambient air over a Reynolds number range of $50 < Re < 900$. Water at 60 °C was circulated through the radiators to maintain a constant fin temperature during the tests. For steady flow, it was found that the heat transfer rate increased linearly with the mass flow rate of air. The pulsatile flow experiments showed that frequency of pulsation had a negligible effect on the heat transfer rate for the range of frequencies tested (0.5 Hz – 2.5 Hz). For all three radiators, the heat transfer rate was decreased in the case of pulsatile flow. Linear heat transfer correlations for steady and pulsatile flow were calculated in terms of Reynolds number and Nusselt number.

Keywords**—**Finned-tube heat exchangers, radiators, heat transfer correlations, pulsatile flow, computer radiators.

I. Introduction

STIRLING engines are currently being investigated for utilization of low-grade heat sources below 150 °C. Heat exchanger design optimization for Stirling engines presents a significant challenge due to unsteady, compressible, flow for which there is limited experimental data. This paper develops linear empirical heat transfer correlations for finned-tube heat exchangers in both steady and pulsatile flows. Although real fluid motion in a Stirling engine is more complex, this research provides a stepping-stone towards its understanding.

Several authors have conducted numerical investigations on the effect of pulsatile flow on heat exchanger performance. Cho and Hyun [1] solved the laminar boundary layer equations numerically for pulsating flow in a circular pipe. They found that the Nusselt number for pulsatile flow can increase or decrease relative to the steady flow value, depending on the pulsation frequency. It was determined by Chattopadhyay et al. [2] that for laminar flow in a circular pipe, pulsation had a negligible effect on the time-averaged heat transfer rate for low frequency and amplitude. For turbulent flow in a circular pipe, numerical results indicated a heat transfer enhancement, at an optimum value of Womersley number, a dimensionless variable which describes the relationship between frequency and viscous forces [3]. Kim et al. [4] considered pulsatile flow in a two-dimensional channel filled with porous media. Their results showed that pulsatile flow decreased the heat transfer rate in the entrance region of the channel and increased it at moderate downstream locations. Further along the channel, the pulsation was ineffectual. They also noted that the pulsatile flow showed the largest deviation from steady flow at large amplitudes and small values of the pulsation frequency parameter. In the case of a curved pipe, the calculations of Chung and Hyun [5] showed that for small Womersley numbers, the Nusselt number was decreased for pulsatile flow. As Womersley number increased, the pulsatile flow Nusselt number approached the steady flow case.

Other authors have also explored pulsatile flow heat exchange experimentally. Habib et al. [6] demonstrated that the Nusselt number enhancement depends strongly on pulsation frequency for a laminar flow of air in a circular pipe. For turbulent flow in a similar geometry, a paper by the same first author reported that the Nusselt number could be increased, decreased, or unchanged relative to the steady flow case, depending on the frequency and Reynolds number [7].

Wantha [8] studied finned tube heat exchangers in steady and pulsatile flows of air. The experiment covered a frequency range of 10 to 50 Hz, and a relative amplitude range of 13.33 to 15.35%. Wantha's results showed that the Nusselt number could be increased relative to steady flow. The increase was greater for higher Reynolds numbers, and each Reynolds number had a unique optimum frequency for Nusselt number enhancement.

This study considers both steady, and pulsatile flow applied to the air side of a computer radiator. The results are applicable to computer cooling system design, and provide insight on unsteady flow heat exchangers in general.

II. Experiment Set-up

A process and instrumentation diagram of the experiment setup is shown in Fig. 1 and compared with an image of the actual experiment in Fig. 2. Air flowed from an accumulation tank, through a mass flow controller (MC500, Cole-Parmer Canada Company) into the experiment duct via a diffuser. The custom 3D printed diffuser expanded the flow geometry from a ¾ in NPT fitting to the rectangular duct and provided a more uniform velocity profile in the duct. The rectangular duct was a 0.61 m long acrylic airflow channel built to test the performance of radiators sized for 120 mm fans. Fig. 3 contains the cross-sectional dimensions of the experiment duct. The radiators examined are the EK-CoolStream XE 120, the EK-CoolStream PE 120, and the EK-CoolStream SE 120 whose dimensions and surface areas are in Table I and

J. P. Michaud, C. P. Speer, and D. A. Miller are M.Sc. candidates in the Department of Mechanical Engineering, University of Alberta, Edmonton, AB T6G 2G8 Canada (e-mail: jpmichau@ualberta.ca, cspeer@ualberta.ca, damiller@ualberta.ca).

D. S. Nobes is a Professor with the Department of Mechanical Engineering, University of Alberta, Edmonton, AB T6G 2G8 Canada (e-mail: dnobes@ualberta.ca).

depicted in Fig. 4. After passing through the radiator, air exited the experiment duct to ambient, through a nozzle. To maintain the radiators near 60 °C, a hot water bath (EX 10, NESLAB) circulated distilled water through the radiator in an open loop.

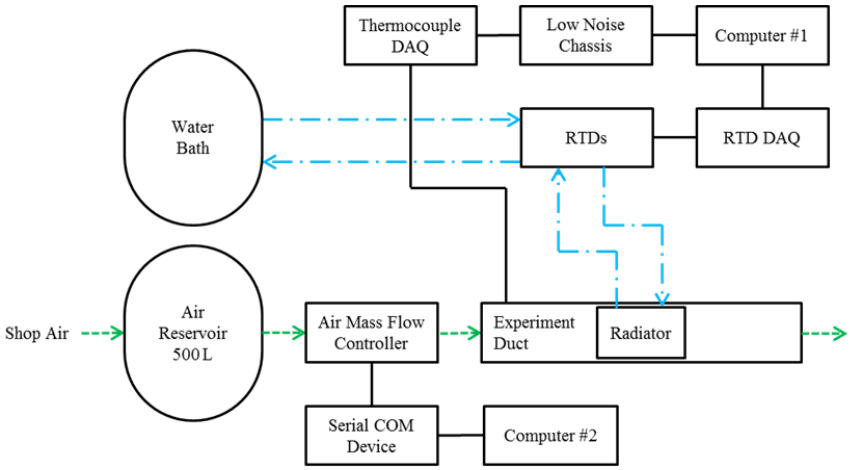

Fig. 1 Process and Instrumentation Diagram of The Radiator Testing Experiment

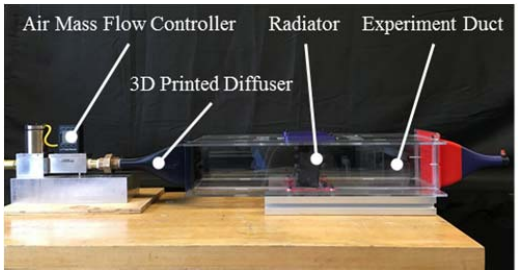

Fig. 2 Image of the Experiment Setup

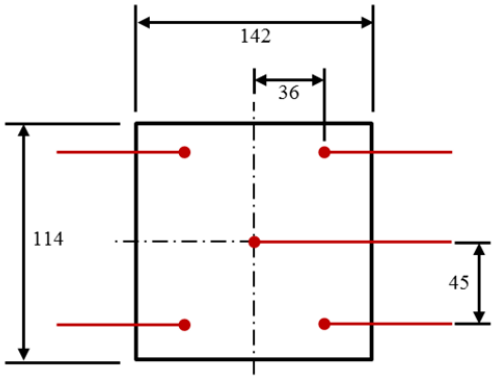

Fig. 3 Cross-Sectional Diagram of Experiment Duct with Thermocouple Locations in Red (dimensions in millimeters)

TABLE I
RADIATOR DIMENSIONS

Radiator	Width (mm)	Height (mm)	Depth (mm)	Heat Transfer Surface Area (cm^2)
XE 120	120	125	46	9319
PE 120	127	114	22	5961
SE 120	114	120	16	3511

A. Temperature Measurement Instruments

Both air and water temperature data were logged for analysis. Exposed junction Type-T thermocouples (TJFT72, Omega Engineering Inc.) measured air temperature in the experiment duct in eleven positions—five immediately before and after the radiator in the locations shown in Fig. 3 and one in the exhaust nozzle. Two RTD probes (RTD-810, Omega Engineering Inc.) measured the water inlet and outlet temperature of the radiator.

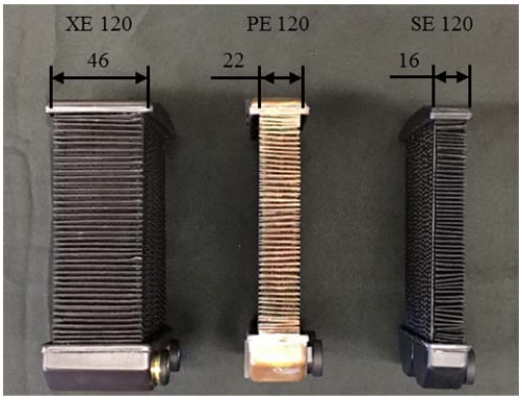

Fig. 4 Images of All Three Radiators with Depth Dimensions (dimensions in millimeters)

B. Data Acquisition

One computer (Comp #1) gathered all the temperature data. The thermocouple data-acquisition-device (TC 2095, National Instruments Inc.) transmitted air temperature data to computer 1 via the NI MAX SCXI 1000 low-noise chassis. The NI 9217 RTD data-acquisition-device transmitted the water temperature data to Comp #1. Comp #1 alternately collected data from each data-acquisition-device at a frequency of 1 Hz.

A second computer (Comp #2) was responsible for the air mass flow controller. Comp #2 commanded the air mass flow controller to change or maintain its set point at a frequency of 10 Hz through a NI USB-232/2 serial COM device. Similarly, the mass flow controller returned volume flow rate, mass flow

rate, temperature, and pressure measurements at a 10 Hz through the serial COM device. Comp #2 logged the command set point and all the flow controller data.

III. Experiment Methodology

TABLE II
NOMENCLATURE

Symbol	Description	Unit
A_{air}	Cross-sectional area of radiators exposed to air	m^2
A_s	Surface area of radiators exposed to air	m^2
$c_{p,}$	Constant pressure specific heat	J/(kg °C)
f	Pulsation frequency	Hz
h	Convective heat transfer coefficient of Air	W/(m^2 °C)
k	Thermal conductivity of air at 40 °C	W/(m °C)
L	Radiator fin depth	m
$\dot{m}$	Air mass flow rate	kg/s
Nu	Nusselt Number	-
$\dot{Q}$	Heat transfer rate	W
Re	Reynolds Number	-
T_{in}	Radiator air inlet temperature	°C
T_s	Radiator surface temperature	°C
v	Average air velocity in radiator	m/s
ΔT	Arbitrary temperature difference	°C
μ	Viscosity of air at 40 °C	kg/(m s)
ρ	Density of air at 40 °C	kg/(m^3)

The responding variables of the experiment are the measured air and water temperature difference. As seen in (1), the heat transfer rate, $\dot{Q}$, may be calculated for each radiator by varying the mass flow rate, $\dot{m}$, and measuring the temperature difference, ΔT, assuming a constant specific heat, c_p such as:

$$\dot{Q} = \dot{m} \cdot c_P \cdot \Delta T \quad (1)$$

For the steady state experiments, the manipulated variables were the radiator surface area and air flow rate. For the pulsatile flow experiments, radiator surface area, pulse frequency and amplitude were the manipulated variables. The internal control system of the water bath maintained the water temperature at 60 °C. Water mass flow rate was determined by weighing six 40 s samples of water circulated through the system for each radiator.

A. Steady Flow Experiments

In the steady flow experiments, constant airflow rates were passed through each radiator in random order. Table III lists the two groups of flow rates that flowed through the radiators. The lower group is from 50 to 100 LPM for comparison with the pulsatile mean airflow rates. The higher group is from 100 to 300 to expand the steady flow data. All 30 experiments were 400 s to ensure sufficient steady state data was gathered.

B. Pulsatile Flow Experiments

The pulsatile flow experiments had pulsating airflow rates passing through each radiator at several frequencies as listed in Table IV. Similarly, to the steady flow experiments, the pulsatile flow experiment was performed in random order with respect to the maximum airflow set point and pulsation frequency. The anticipated mean pulsatile airflow rates correspond to the lower group of steady state flow rates. Equipment limitations restricted the range of airflow set points and pulsation frequencies available for analysis. Again, all 90 experiments were 400 s long to ensure enough data was collected at thermal steady state.

TABLE III
STEADY FLOW MANIPULATED VARIABLES

Number	Air Flow Rate Set point (LPM)
1	50
2	60
3	70
4	80
5	90
6	100
7	150
8	200
9	250
10	300

TABLE IV
PULSATILE FLOW MANIPULATED VARIABLES

Number	Air Flow Rate Setpoint Maximum (LPM)	Pulsation Frequency (Hz)
1	100	0.5
2	120	1.0
3	140	1.5
4	160	2.0
5	180	2.5
6	200	-

IV. Data Processing

Heat transfer rate, convective heat transfer coefficient, Reynolds number and Nusselt number characterize the performance of radiators. The calculations used constant properties of air at 40 °C and atmospheric pressure. Furthermore, calculations applied mean air mass flow rate data averaged over the entire dataset. Calculations requiring temperatures used the mean temperature averaged beyond data point 300 (approximately 300 s) to ensure the thermally transient portion of the data was ignored.

Fig. 5 presents a sample of the raw data collected for the inlet and outlet temperatures for both steady and pulsatile flows. Both the steady flow and pulsatile flow samples stabilize after approximately 300 s.

The average air velocity, v, through the radiator was calculated using:

$$v = \frac{\dot{m}}{(\rho \cdot A_{air})} \quad (2)$$

where the air mass flow rate is $\dot{m}$, the density of the air is ρ, and the surface area of the radiator exposed to air is A_{air}.

The Reynolds number, Re, for the air was then calculated using:

$$Re = \frac{\rho \cdot v \cdot L}{\mu} \quad (3)$$

where μ is the dynamic viscosity of air, and L is the characteristic length scale, which was assumed to be the length of the fins in the flow direction [9].

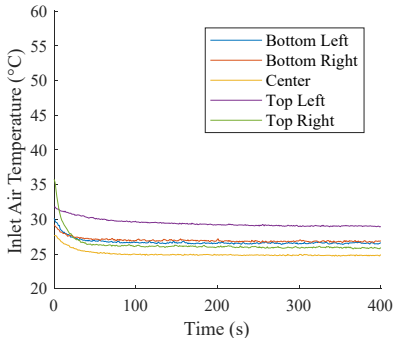

(a)

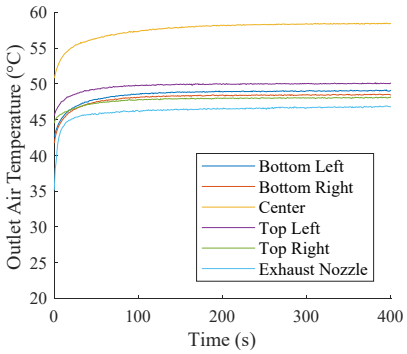

(b)

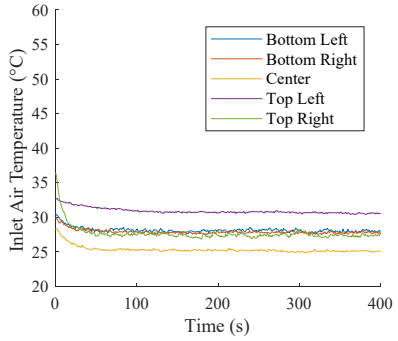

(c)

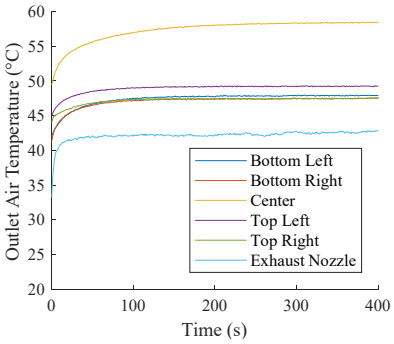

(d)

Fig. 5 Raw data plots of (a) the steady flow inlet air temperature and (b) outlet air temperature through radiator XE 120 with a set point of 70 LPM; and (c) raw data plots of pulsatile flow inlet air temperature (d) and outlet air temperature through radiator XE 120 with a maximum set point of 140 LPM at a pulsation frequency of 1.0 Hz

The convective heat transfer coefficient, h, was calculated using:

$$h = \frac{\dot{Q}}{(A_s \cdot (T_s - T_{in}))} \quad (4)$$

with the heat transfer rate from (1), surface area of each radiator, A_s, shown in Table I, the radiator surface temperature, T_s, which was measured to be approximately 59 °C, and the averaged air inlet temperature, T_{in}.

The Nusselt number, Nu, was calculated for a thermal conductivity k is the of the air using:

$$Nu = \frac{h \cdot L}{k} \quad (5)$$

V. Results and Discussion

Fig. 6 is a plot of heat transfer rate with respect to mean mass flow rate for all three radiators. As expected, the heat transfer rate increases with an increase in mass flow rate. Additionally, the XE 120 radiator, with the largest surface area, has a greater heat transfer rate followed by the PE 120, and SE 120.

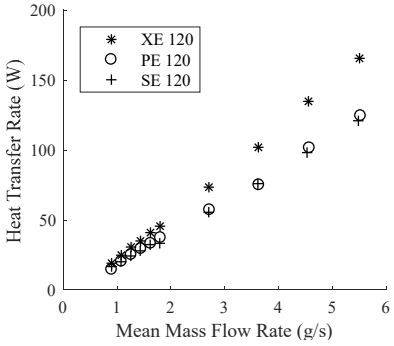

Fig. 6 Plot Comparing Steady Flow Heat Transfer Rate and Mean Mass Flow for Each Radiator

Fig. 7 shows the steady and pulsatile heat transfer rates for the XE 120 radiator. The graph indicates that the performance of the radiator is superior for steady flow compared to pulsatile flow. However, the advantage is not distinct since both data sets nearly collapse to a straight line. In addition, the frequency of pulsation did not have a significant effect on the heat transfer rate for the frequency range of 0.5 Hz to 2.5 Hz.

Fig. 8 demonstrates the heat transfer rate as a function of average mass flow rate for the PE 120 radiator. The results indicate that the performance of the radiator is also decreased by the pulsatile flow. However, similar to the XE 120, the pulsatile and steady data are not significantly different in terms of performance enhancement.

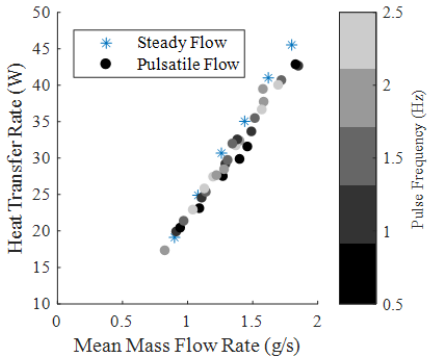

Fig. 7 Plot Comparing Heat Transfer Rate and Mean Mass Flow for Steady and Pulsatile Flows for the EK XE 120

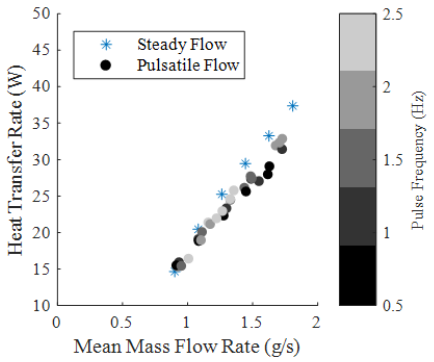

Fig. 8 Plot Comparing of Heat Transfer Rate and Mean Mass Flow for Steady and Pulsatile Flows for the EK PE 120

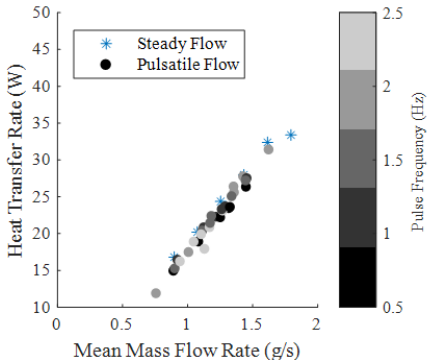

Fig. 9 Plot Comparing of Heat Transfer Rate and Average Mass Flow for Steady and Pulsatile Flows for the EK SE 120

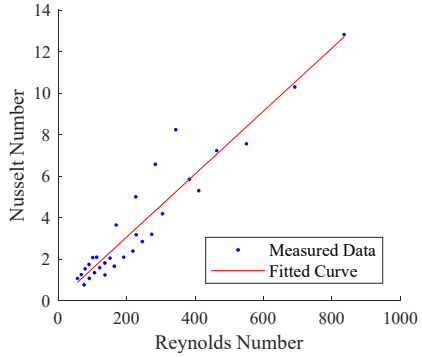

Fig. 10 Plot Correlating Steady Flow Nusselt Number and Reynolds Number

Similar to the XE and PE radiator the SE 120 radiator also has a decreased heat transfer rate under pulsatile flow conditions. Data supporting this is presented in Fig. 9.

Figs. 7-9 indicate that, for the conditions tested here, pulsatile flow has a negative effect on the rate of heat transfer from finned-tube radiators tested.

Fig. 10 shows the Nusselt number correlation for steady flow conditions. Three distinct lines of data are visible, corresponding to the three radiators tested. The separation of the three lines can be attributed to the geometric differences between the three radiators. The Reynolds number, as calculated here, does not overcome the differences in fin structure and tube layout that exist between the three radiators. A linear polynomial fit was calculated to produce the Nusselt number correlation for steady flow, shown in (6). The R^2 value for the linear fit was 0.904.

$$Nu = 0.01517 \cdot Re + 0.3523 \quad (6)$$

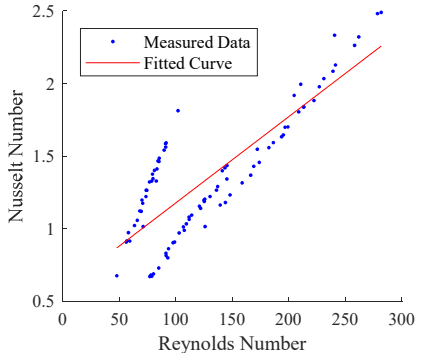

Fig. 11 Plot Correlating Pulsatile Flow Nusselt Number and Reynolds Number

Fig. 11 corresponds to pulsatile flow. The Reynolds number was based on the average flow velocity through the radiator. The R^2 value was 0.6968, indicating a poor fit relative to the steady flow case. Similarly, three distinct lines can be seen in Fig. 11, which indicate that the Reynolds number definition did not adequately capture the geometric differences between the radiators. A more detailed dimensionless number would be required to improve the fit. The correlation equation for pulsatile flow is shown in (7):

$$Nu = 0.00594 \cdot Re + 0.5850 \quad (7)$$

VI. Conclusions and Future work

The heat transfer performances of three finned-tube heat exchangers in both steady and pulsatile flows were investigated. The results of this study indicate that pulsatile flows decrease heat transfer rates for the range of geometries and flow conditions tested.

Future work would include testing a wider range of flow conditions, including oscillating flow and compressible flow, to better represent flows present in low temperature Stirling engines. The pressure drop across the radiators should also be correlated to facilitate design optimization. Additionally, different dimensionless numbers and characteristic length scales should be explored to produce more universal design plots.

Acknowledgment

This work was conducted with the support of the Natural Sciences and Engineering Research Council (NSERC) of Canada, the Canadian Foundation of Innovation (CFI), Alberta Innovates Energy and Environment Solutions, and Terrapin Geothermics. Micheal Bayans, Carlos Mendez, and Jakub Piwowarczyk provided advice and equipment support.

References

[1] H. W. Cho and J. M. Hyun, "Numerical solutions of pulsating flow and heat transfer characteristics in a pipe," *Int. J. Heat Fluid Flow*, vol. 11, no. 4, pp. 321–330, 1990.

[2] H. Chattopadhyay, F. Durst, and S. Ray, "Analysis of heat transfer in simultaneously developing pulsating laminar flow in a pipe with constant wall temperature," *Int. Commun. Heat Mass Transf.*, vol. 33, no. 4, pp. 475–481, 2006.

[3] X. Wang and N. Zhang, "Numerical analysis of heat transfer in pulsating turbulent flow in a pipe," *Int. J. Heat Mass Transf.*, vol. 48, no. 19–20, pp. 3957–3970, 2005.

[4] S. Kim, B. Kang, and J. Hyun, "Heat transfer in the thermally developing region of a pulsating channel flow," *Int. J. Heat Mass Transf.*, vol. 36, no. 17, pp. 4257–4266, 1993.

[5] J. Chung and J. Hyun, "Heat transfer from a fully-developed pulsating flow in a curved pipe," *Int. J. Heat Mass Transf.*, vol. 37, no. 1, pp. 43–52, 1994.

[6] M. A. Habib, A. M. Attya, A. I. Eid, and A. Z. Aly, "Convective heat transfer characteristics of laminar pulsating pipe air flow," *Heat Mass Transf.*, vol. 38, no. 3, pp. 221–232, 2002.

[7] M. A. Habib, S. A. M. Said, A. A. Al-Farayedhi, S. A. Al-Dini, A. Asghar, and S. A. Gbadebo, "Heat transfer characteristics of pulsated turbulent pipe flow," *Heat Mass Transf.*, vol. 34, no. 5, pp. 413–421, 1999.

[8] C. Wantha, "Effect and heat transfer correlations of finned tube heat exchanger under unsteady pulsating flows," *Int. J. Heat Mass Transf.*, vol. 99, pp. 141–148, 2016.

[9] M. Carl, D. Guy, B. Leyendecker, A. Miller, and X. Fan, "The Theoretical and Experimental Investigation of the Heat Transfer Process of an Automobile Radiator," in *ASEE Gulf Southwest Annual Conference*, 2012, vol. 1, no. 128, pp. 1–12.

Jason P. Michaud is from Sherwood Park, Alberta, Canada, and is a MSc. Candidate in the Department of Mechanical Engineering at the University of Alberta, Edmonton, Alberta, Canada. He completed his BSc. of mechanical engineering in 2016 at the same institution.

Connor P. Speer is an MSc Candidate in the Department of Mechanical Engineering at the University of Alberta in Edmonton, Alberta, Canada. He completed a BSc. In Mechanical engineering in 2015 at the same institution.

David A. Miller was raised in St. Paul, Alberta, Canada. He completed a BSc. of mechanical engineering at the University of Alberta, Edmonton, Alberta, Canada in 2016. His is currently a MSc. Candidate in the Department of Mechanical Engineering at the University of Alberta.

David S. Nobes has a BE and PhD in mechanical engineering from the University of Adelaide, Australia. He is now a Professor in the Department of Mechanical Engineering at the University of Alberta, Canada.